Check for updates

Received: 21 January 2023 | Revised: 20 June 2023 | Accepted: 22 June 2023

DOI: 10.1002/ar.25289

SPECIAL ISSUE ARTICLE

The Anatomical Record WILEY

A preliminary analysis of dental microstructure in *Hamipterus* (Pterosauria, Pterodactyloidea)

He Chen[1,2,3] | Zhiheng Li[3] | Shunxing Jiang[3] | Qian Wu[3,4] | Yanxin Gong[5] | Xufeng Zhu[6] | Xiaolin Wang[3,4]

[1]School of Ecology, Sun Yat-sen University, Shenzhen, China

[2]The Museum of Biology, Sun Yat-sen University, Guangzhou, China

[3]Key Laboratory of Vertebrate Evolution and Human Origins, Institute of Vertebrate Paleontology and Paleoanthropology, Chinese Academy of Sciences, Beijing, China

[4]University of the Chinese Academy of Sciences, Beijing, China

[5]Shenzhen Museum, Shenzhen, China

[6]National Natural History Museum of China, Beijing, China

Correspondence

Xiaolin Wang, Key Laboratory of Vertebrate Evolution and Human Origins, Institute of Vertebrate Paleontology and Paleoanthropology, Chinese Academy of Sciences, Beijing, 100044, China.
Email: wangxiaolin@ivpp.ac.cn

Funding information

National Natural Science Foundation of China, Grant/Award Numbers: 41572020, 42072028, 42288201; Strategic Priority Research Program (B) of CAS, Grant/Award Number: XDB26000000; Youth Innovation Promotion Association of the Chinese Academy of Sciences, Grant/Award Number: 2019075

Abstract

The toothed members of Pterosauria display an extremely wide range of tooth morphologies that supported a variety of feeding habits. Histological studies on the teeth of different pterosaur clades are potentially valuable in understanding the development of their tooth diversity. In this study, we used histological sections and scanning electron microscopy to describe and interpret the tooth microstructure of *Hamipterus* (Pterodactyloidea). Our analysis is based on seven teeth of *Hamipterus* (six isolated and one from a skull) from the Lower Cretaceous collected in Hami, China. Our results show that the enamel on the tooth crown is thin (~25 μm) in *Hamipterus* and covers only approximately half of the tooth crown. This thin enamel of the *Hamipterus* tooth makes it vulnerable and often becomes damaged during taphonomic and diagenetic processes. The radicular pulp inside the conical-shaped root shows a spindle space with a small foramen at the bottom, while the coronal pulp shows a small tunnel (100–140 μm in diameter). We estimate that the small teeth of *Hamipterus* likely took approximately 80 days to form. Furthermore, the tooth has Andresen lines, which represent 7–15 days period. For stable articulation of the tooth in the alveolus, the thick cellular cementum is concentrated on the lingual side of the root. The acellular cementum (~40 μm thick) layer runs from the root to the partial tooth crown.

KEYWORDS

dental microstructure, *Hamipterus*, histology, pterosaurs, tooth formation time

1 | INTRODUCTION

Fossil teeth are one of the most popular materials applied in biochronology, environmental and ecological characterization (via isotopic analysis of the enamel), and evolutionary studies because of the valuable information recorded therein (Bestwick et al., 2018; Gong et al., 2020; Kundanati et al., 2019). As a large group of extinct flying reptiles that once ruled the Mesozoic sky, pterosaurs exhibit a wide range of tooth morphotypes (Bestwick et al., 2018; Chiappe et al., 2000; Dalla Vecchia, 2004; Fastnacht, 2001; Fröbisch & Fröbisch, 2006; Ősi, 2011). Since the 19th century (Owen, 1845), diverse tooth morphotypes of pterosaurs have been reported, and their variation has been used to reconstruct their phylogeny, inferring dietary and feeding ecologies (e.g., Benton et al., 2000; Bestwick et al., 2018; Kellner & Mader, 1997; Martill et al., 2023; Ősi, 2011; Sánchez-Hernández

 © 2023 American Association for Anatomy.

et al., 2007; Xu et al., 2022; Zhou et al., 2017). However, the basic tooth microstructure of pterosaurs has been minimally analyzed (Cerda & Codorniú, 2023; Fastnacht, 2008; Vidovic, 2010), which is important for solving discrepancies regarding structure and obtaining more biological information (Cerda & Codorniú, 2023).

In addition to the importance of the basic architecture of the tooth, several histological studies of other archosaur teeth have also provided insights into the feeding behavior and paleoecology of extinct organisms (Brink et al., 2015; D'Emic et al., 2019; Fiorillo & Currie, 1994; Heckeberg & Rauhut, 2020) and the competitive strategies derived from tooth microstructure (Li et al., 2020). Histological thin sections of the teeth in crocodylians were used in the calculation of tooth formation time by counting the incremental lines of von Ebner in the dentine (Erickson, 1996a, 1996b). Improved methods have also been widely applied to calculate the tooth formation time and replacement rates of dinosaurs (e.g., Button et al., 2017; D'Emic et al., 2013; D'Emic et al., 2019; Erickson, 1996b; Kosch & Zanno, 2020; Ősi et al., 2022; Sereno et al., 2007).

Although a few studies have focused on the histological teeth of pterosaurs (Cerda & Codorniú, 2023; Vidovic, 2010), the complex and varied results already imply their value for their different biological information. ?*Santanadactylus* sp. (Pterodactyloidea) has a plesiomorphic enamel microstructure compared to that of other archosaurs (Vidovic, 2010). *Pterodaustro*, from another clade of Pterodactyloidea, differs from ?*Santanadactylus* sp. in having a filamentous tooth in the aulacodont condition (Cerda & Codorniú, 2023). Therefore, to understand the dental variation and complexity in the evolution of pterosaurs, extensive research on the basic dental microstructure of different clades is necessary. Recently, the Lower Cretaceous Shengjinkou Formation of the Tugulu Group in Hami, China, has yielded a large number of three-dimensionally preserved bones of *Hamipterus tianshanensis*, including three-dimensionally preserved male and female skulls with teeth and eggs (Wang et al., 2014, 2017, 2020). The adult individual has 19 teeth in the upper jaw and 15 teeth in the lower jaw on each side with variation in size, position, and morphology (Wang et al., 2014). The tooth crowns range from large, anterolaterally inclined, and lance-shaped to smaller, vertical, and more posteriorly triangular, but they are all laterally flattened and medially curved with smooth labial and fluted lingual enamel surfaces (Wang et al., 2014). Although the morphology of the teeth has been well described, the basic internal microstructure of the tooth in *Hamipterus* is not fully understood. In addition, the fossil teeth of *Hamipterus* are typically not the toughest part of the skeleton. They are very fragile like other fossil bones, easily broken apart and often missing the crown. To understand this phenomenon and shed light on the development of the diverse tooth morphologies of pterosaurs, we describe and interpret the microstructure of *Hamipterus* teeth using both scanning electron microscopy (SEM) and polarizing light microscopy. We find limited coverage of thin enamel in *Hamipterus*, which is often not well preserved. We also estimate the tooth formation time of *Hamipterus* using von Ebner lines in the orthodentine.

2 | MATERIALS AND METHODS

2.1 | Specimens and methods

Six isolated teeth (IVPP V 32250.1–32250.6) and one tooth (IVPP V 32251.1) from the skull (IVPP V 32251) of *Hamipterus* were selected to study tooth microstructure. All teeth belong to the *Hamipterus* specimens that were recovered from our fieldwork at the fossil site of *Hamipterus* in Hami, China (Wang et al., 2014), and deposited at the Institute of Vertebrate Paleontology and Paleoanthropology (IVPP), Chinese Academy of Sciences. Only IVPP V 32250.6 had a preserved tooth crown, while the other six teeth lacked the tip (Figures 1–3). To investigate the microstructure of *Hamipterus* by SEM and polarizing microscopy, we processed the seven teeth using two methods, with four teeth sliced into thin sections (IVPP V 32250.3–32250.6, Table 1) and the other three (IVPP V 32250.1, 32250.2 and 32251.1) directly examined at their broken surfaces. The high-resolution images show the detail of the structure in the teeth of *Hamipterus*.

2.1.1 | Terminology

The terminology in this study follows Berkovitz and Shellis (2017).

The specimens were prepared and examined in the following laboratories and institutes:

Chinese Academy of Sciences, China (CAS);
Key Laboratory of Vertebrate Evolution and Human Origins, Institute of Vertebrate Paleontology and Paleoanthropology, Beijing, China (IVPP);
China Geological Survey, Beijing, China (CGS);
Museum of Biology, Sun Yat-sen University Mawenhui Hall, Guangzhou, China (SYSU-MB);
School of Materials Science and Engineering, Sun Yat-sen University, Guangzhou, China (SYSU-MSE).

19328494, 0, Downloaded from https://anatomypubs.onlinelibrary.wiley.com/doi/10.1002/ar.25289 by INST VERTEBRATE PALEONANTOLOGY, Wiley Online Library on [08/08/2023]. See the Terms and Conditions (https://onlinelibrary.wiley.com/terms-and-conditions) on Wiley Online Library for rules of use; OA articles are governed by the applicable Creative Commons License

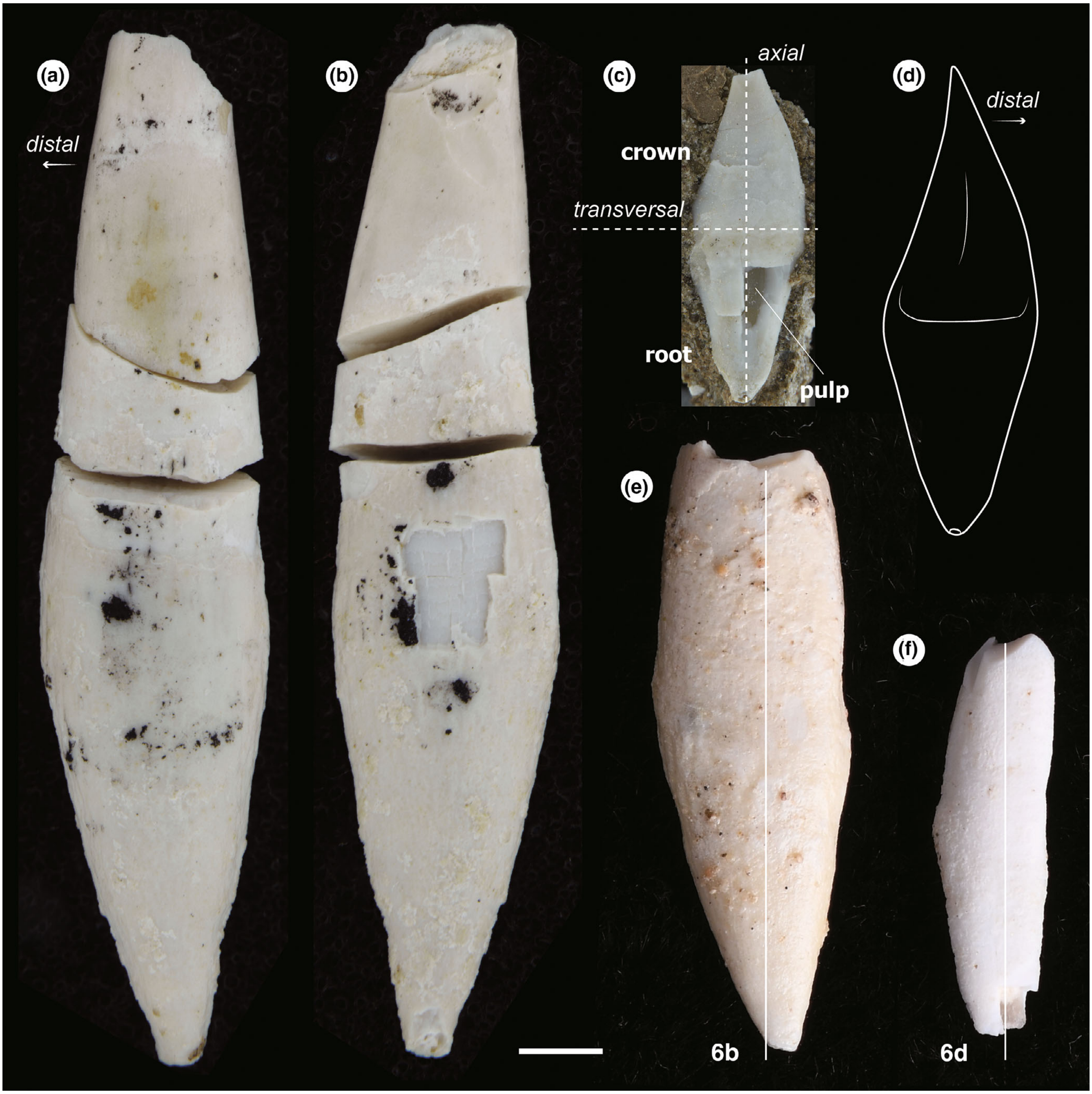

FIGURE 1 Variety of isolated *Hamipterus* teeth from the Lower Cretaceous Shengjinkou Formation of the Tugulu Group in Hami, China. (a) and (b) are IVPP V 32250.1 in labial (a) and lingual (b) views. Photo (c) and line drawing (d) of IVPP V 32250.2 in lingual view, and (d) is not in scale. (e) and (f) are IVPP V 32250.3. and 32250.4 in the labial view, respectively. The lines labeled 6b,d correspond to the locations of the axial section cuts shown in Figure 6b,d, respectively. Scale bar: 2 mm.

2.1.2 | Sample preparation

To directly examine the broken surface by SEM, the samples were cleaned by an air duster. We focus on the broken surfaces from IVPP V 32250.1 (Figure 1a,b, broken into three parts), the smallest tooth (IVPP V 32250.2, Figure 1c) and the tooth root (IVPP V 32251.1, Figure 2) from the skull (IVPP V 32251). The other four teeth (IVPP V 32250.3–32250.6) were sliced after being epoxy-embedded in the laboratory at IVPP. These four tooth samples were embedded in EXAKT Technovit 7200 one-component resin. They were cut longitudinally (IVPP V 32250.3–32250.6, Table 1) using the EXAKT 300CP cutting system, and one (IVPP V 32250.5) was also cut transversally. The thin sections were ground and polished to a thickness of approximately 50–60 μm using an EXAKT 400CS variable-speed grinding system with P500 and P4000 abrasive papers.

19328494, 0, Downloaded from https://anatomypubs.onlinelibrary.wiley.com/doi/10.1002/ar.25289 by INST VERTEBRATE PALEONANTOLOGY, Wiley Online Library on [08/08/2023]. See the Terms and Conditions (https://onlinelibrary.wiley.com/terms-and-conditions) on Wiley Online Library for rules of use; OA articles are governed by the applicable Creative Commons License

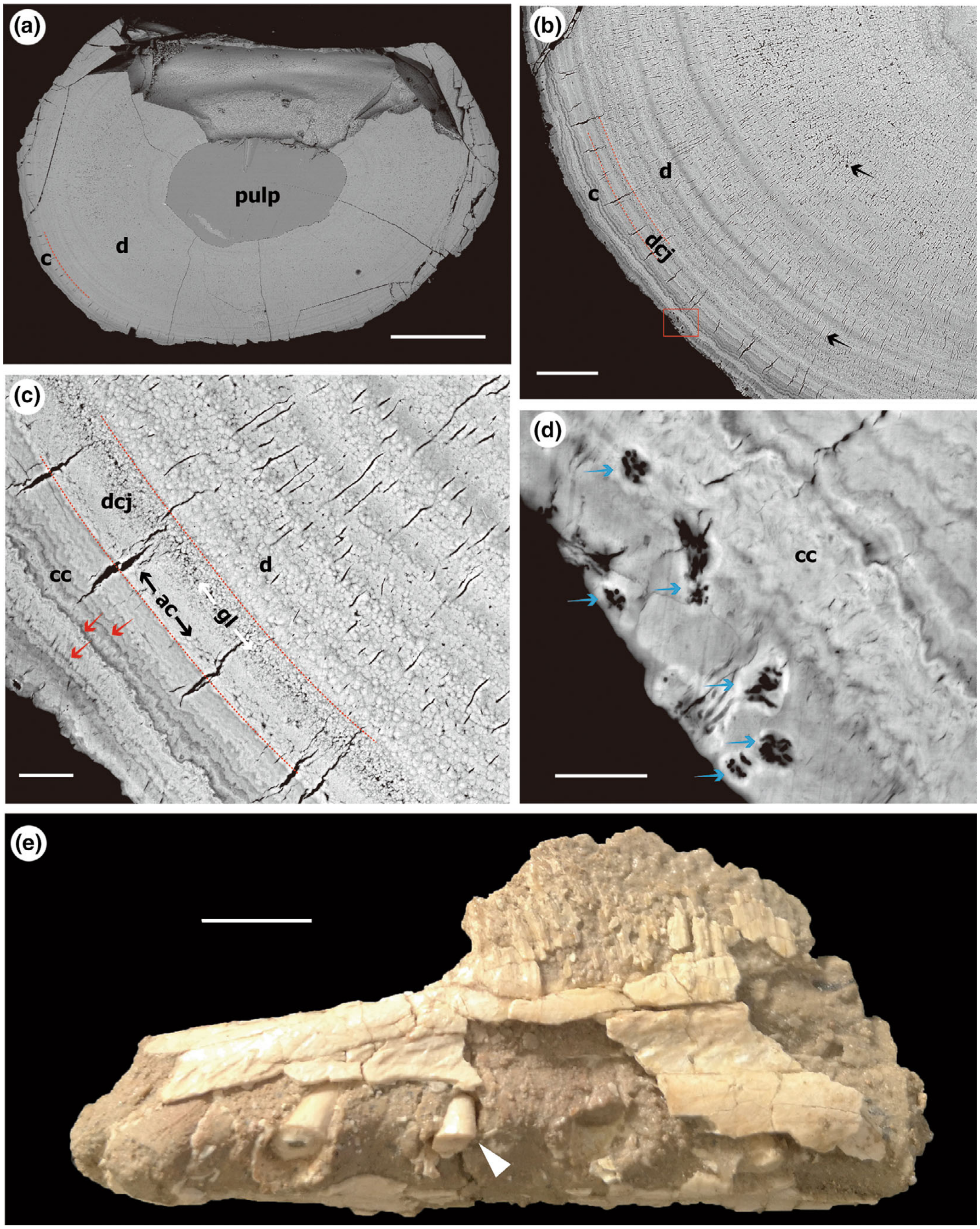

FIGURE 2 SEM micrographs of the dental structure on the transverse broken surface of *Hamipterus* (IVPP V 32251.1). (a) is the transverse section of the root area. (b) is the close-up of (a) with different tubule lacunae in the dentine area. (c) shows the dentine–cementum junction area. The acellular cementum layer is deposited over a thin granular layer of dentine, and the arrest lines (red arrow) are clear in the cellular cementum as the last layer on the root. (d) is a close-up of the red box in (b) that shows the clusters of cementocyte lacunae (blue arrow) embedded in cellular cementum. (e) shows where tooth IVPP V 32251.1 was positioned in the skull of *Hamipterus* IVPP V 32251. ac, acellular cementum; c, cementum; cc, cellular cementum; d, dentine; dcj, dentine–cementum junction; gl, granular layer. Scale bars: a = 500 μm, b = 100 μm, c = 20 μm, d = 10 μm, e = 1 cm.

2.1.3 | Scanning electron microscopy, energy dispersive x-ray spectroscopy (EDS) (SEM–EDS) and polarizing microscopy

We used Phenom Pro SEM at SYSU-MB to observe and image the broken surfaces of the teeth of IVPP V 32250.1–32250.2 with a voltage of 10 kV. The Zeiss BK-POL polarized light microscope at SYSU-MSE and Zeiss Axio Imager A2 polarized light microscope at IVPP were used to study the thin sections (IVPP V 32250.3–32250.6). The Zeiss MA EVO25 SEM at IVPP was used for analyzing the thin sections of IVPP V 32250.3, 32250.4 and 32250.6 under a 20 kV

19328494, 0, Downloaded from https://anatomypubs.onlinelibrary.wiley.com/doi/10.1002/ar.25289 by INST VERTEBRATE PALEONTOLOGY, Wiley Online Library on [08/08/2023]. See the Terms and Conditions (https://onlinelibrary.wiley.com/terms-and-conditions) on Wiley Online Library for rules of use; OA articles are governed by the applicable Creative Commons License

acceleration voltage after vacuum sputter coating in gold palladium. Two thin sections (IVPP V 32250.3 and 32250.4) were etched in 5% hydrochloric acid (20 s), subjected to an ultrasonic bath, and air-dried for SEM and EDS. The FEI Quanta 450 SEM at CGS was used to analyze the thin sections of IVPP V 32250.5 and broken surface of IVPP V 32251.1 with a voltage of 20 kV and EDS.

2.1.4 | Photography and drawings

Each specimen photograph and drawing were edited and completed by Adobe Creative suite 3 design standard in IVPP.

3 | RESULTS

3.1 | Gross description

The tooth of *Hamipterus* can be divided into the crown and the root, similar to other archosaur teeth (Figure 1). All fossil teeth of *Hamipterus* are very fragile, with extensive development of transverse and sagittal cracks (Figure 1). The roots of these teeth are often better preserved than the crown, with little or no damage to the root tip (Figures 1, 2 and 4). Sagittal cracks on the surface of every tooth crown are relatively small (Figure 5g). The ontogenetic stage cannot be determined based on these isolated teeth (Figures 1, 2 and 4). However, the relative positions of the four isolated teeth along the tooth line are clear (Table 1), corresponding to the variable length and size of the tooth crown at different positions along the tooth row (Wang et al., 2014). The long lance-shaped teeth (IVPP V 32250.1, 32250.3 and 32250.4) are positioned closer to the rostrum, while the conical-shaped tooth (IVPP V 32250.2) is posterior to the mandibular symphysis if the tooth is located in the mandible. The axial length of the crown is either greater than (Figure 1a) or similar to that of the root (Figure 1c). The lingual side of the crown is concave, and the crown is also slightly concave on the mesial side (Figure 1d). The root of the tooth has a rough surface and is slightly curved to the lingual side. However, its outer surface is not as lingually concave as the crown. A conical shaped tooth root is commonly observed in other sharp-toothed pterosaurs (Fastnacht, 2001) and has been observed in the Triassic pterosaur group, including species such as *Eudimorphodon* cf. *ranzii* (Wellnhofer, 2003).

A slender cavity tunnel is centrally present as the coronal pulp, with a relatively constant diameter of 130–136 μm in IVPP V 32250.1 (Figure 5b,c) and 49 μm in IVPP V 32250.2. In contrast, the root has a larger pulp cavity with a spindle shape (Figures 1c and 6b,c). Furthermore, the labiolingually flattened tooth morphology is also reflected in this radicular pulp (Figure 2a). Unlike the hollow root with a large opened radicular pulp in *Crocodylus* (Enax et al., 2013), the conical-shaped root in *Hamipterus* retains only a very small foramen (~60 μm) for connection of the radicular pulp (Figure 5i).

3.2 | Dental histology

There should be an outer layer of thin enamel covering the tooth crown, as evidenced by the longitudinal section of IVPP V 32250.4 (Figure 7) and V 32250.6 (Figure 3). However, we failed to find any obvious enamel on the tip of the crown (Figure 3), as in ?*Santanadactylus* sp. (Vidovic, 2010). The preserved outer layer of tooth IVPP V 32250.6 is separated from the dentine, as observed through the microscope (Figure 3) and with SEM, and it measures approximately 15–25 μm in thickness. Additionally, SEM images reveal a very thin enamel layer (~8 μm) of tooth IVPP V 32250.2 (Figure 5d), distinguishing it from the dentine in the broken top crown area. While examining the continuous outer layer on the lingual side of the middle crown of IVPP V 32250.3 and 32250.4 (Figures 6b,d and 7), it was challenging to distinguish the boundary between the enamel and the cementum on the outer layer. This difficulty arises due to their similar densities on the intermittent outer surface, as observed through SEM and microscopy. However, as indicated by different polarizing microscopy results on the lingual side of the IVPP V 32250.4 tooth (Figure 7d), there might be a gradual reduction of the enamel layer, which is gradually covered by a thin cementum. Therefore, in contrast to that in ?*Santanadactylus* sp., the enamel in *Hamipterus* covers a larger portion of the crown, likely extending over half of the total functional tooth height (Figure 6a).

The dentine itself contains dense networks (~8 per 10 μm^2) of dentine tubules (Figure 5f). These dentine tubules were observed in all teeth in both the axial and transversal planes (Figures 4–6). Subsurface structures show a dense network of dentine tubules radiating out from an undivided pulp cavity to the surface structures (Figure 5b,f). The SEM image of the fractured teeth revealed that the mineral phase of dentine consists of lamellar-shaped crystallites (Figure 5h). In the transverse plate (Figure 5d,f) of the outer layers in the early mineralized stage, the dentine tubules often appear as tiny, pointed shapes. However, as the root area forms, the dentine tubules exhibit short lines in the outer layers on the transverse plane (Figures 2c and 4g). In the middle

19328494, 0, Downloaded from https://anatomypubs.onlinelibrary.wiley.com/doi/10.1002/ar.25289 by INST VERTEBRATE PALEONANTOLOGY, Wiley Online Library on [08/08/2023]. See the Terms and Conditions (https://onlinelibrary.wiley.com/terms-and-conditions) on Wiley Online Library for rules of use; OA articles are governed by the applicable Creative Commons License

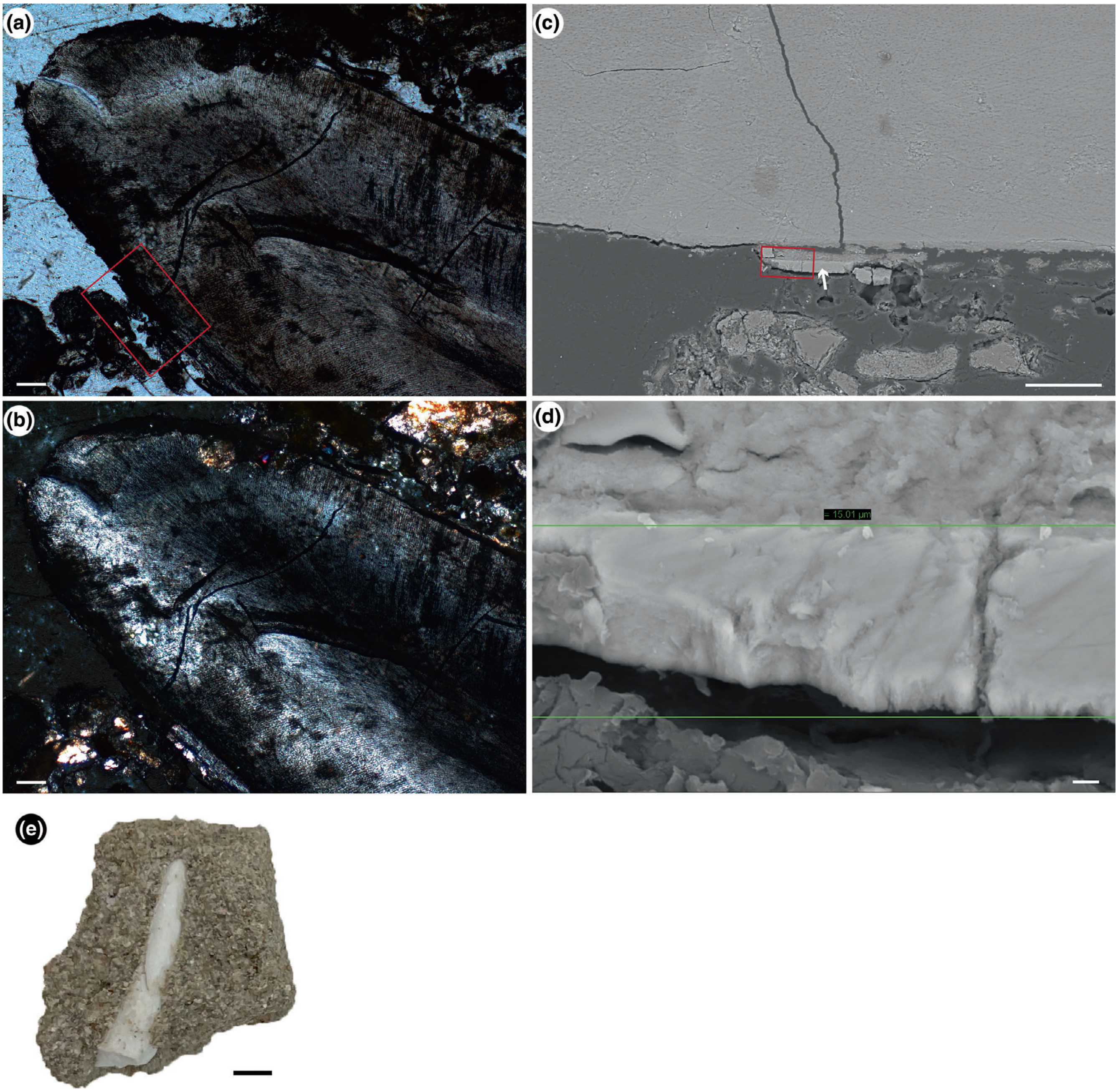

FIGURE 3 Tooth axial micrographs of *Hamipterus* (IVPP V 32250.6). (a) is an axial thin-section micrograph showing the tooth tip of IVPP V 32250.6. (b) is a polarizing micrograph of (a). The SEM micrograph (c) is a close-up of the red box in (a), showing a different outer layer that should represent the enamel (indicated by an arrow). (d) is an SEM micrograph of the enamel, showing increased magnification of the red box in (c). (e) is the tooth IVPP V 32250.6 only preserved crown part. Scale bar: a, b and c = 100 μm, d = 2 μm, e = 2 mm.

layers, the dentine tubules resemble short lines (Figures 2b, 4b,e, and 5c,e), curving toward the radicular pulp (Figures 4a,f and 6b,d). Closer to the pulp, very few dentine tubules are embedded in the last layers (Figures 4b, 5a,b,c). The nontransparent dots in the dentine (Figure 4b) appear to be rather bright in the SEM image (backscatter mode), indicating the intrusion of diagenetic minerals as in its nondental bones (Li et al., 2021).

The transitional region from dentine to enamel is not well preserved. However, on the root, the transition between dentine and cementum is clearly marked by the dentine–cementum junction (dcj). This layer is clearly visible in the SEM images of axially polished sections through the teeth (Figure 6b,d). Similar to those in *Caiman sclerops* (Reptilia, Crocodylidae) (Berkovitz & Shellis, 2017), the dentine tubules terminate at the dcj in the immediately underlying region. In this area, the

19328494, 0, Downloaded from https://anatomypubs.onlinelibrary.wiley.com/doi/10.1002/ar.25289 by INST VERTEBRATE PALEONANTOLOGY, Wiley Online Library on [08/08/2023]. See the Terms and Conditions (https://onlinelibrary.wiley.com/terms-and-conditions) on Wiley Online Library for rules of use; OA articles are governed by the applicable Creative Commons License

TABLE 1 Details of the specimens used for histological study, and tooth formation times counted on the dentine in *Hamipterus*.

Inventory number	Tooth position	Complete tooth root length (mm) * estimated	The tooth width of the mesiodistal widest area (mm)	Tooth formation time (estimated days)	Mean width of von Ebner incremental bands (μm) * lingual/labial	Direction of section/ broken surface	Methods
IVPP V 32250.1	Closer to the anterior of the tooth line	~10.3	~5.5	?	-	Transverse	SEM
IVPP V 32250.2	Closer to the posterior of the tooth line	~3.9	~2.8	?	-	Longitudinal & Transverse	SEM
IVPP V 32250.3	Closer to the anterior of the tooth line	~7.7	~4.8	?	-	Longitudinal	Microscope + SEM + EDS
IVPP V 32250.4	Closer to the anterior of the tooth line	~6.1	~2.7	~80	-	Longitudinal	Microscope + SEM + EDS
IVPP V 32250.5	Closer to the posterior of the tooth line	?	~3.6	?	18.5	Longitudinal & Transverse	Microscope + SEM + EDS
IVPP V 32250.6	Closer to the anterior of the tooth line	?	?	?	?	Longitudinal	Microscope + SEM
IVPP V 32251.1	?	?	~2.5	?	23.5	Transverse	SEM

Note: * estimated; ? unclear.

packing density of the crystallites increases, distinguished as a granular layer (Figure 2c). In the ground sections of IVPP V 32250.5 (Figure 4b,g), the granular layer appears dark and speckled because the light is scattered by the broken and filled matrix during taphonomic processes in numerous spaces, which is caused by incomplete mineralization (Berkovitz & Shellis, 2017).

An acellular layer (Figure 4a) of calcium phosphate surrounds the granular layer of dentine and lacks tubules of uniform thickness (~40 μm). This layer extends from the root to the partial tooth crown (Figure 6b,d) and is surrounded by a thick layer of cellular cementum at the beginning of the root area. Similar to that in crocodylians (Berkovitz & Shellis, 2017; Enax et al., 2013), this acellular layer in *Hamipterus* is likely the acellular cementum layer, considering the typical arrangement of dentin structure. From the outer surface inward, the mineral phase of this acellular layer is not clearly structured in terms of irregularly arranged crystallites (Figures 2c and 4g), which conforms to the loose network of randomly arranged organic fibers in the cementum (Berkovitz & Shellis, 2017). Based on different polarizing microscopy results, the enamel layer is covered by a thin cementum on the lingual side of IVPP V 32250.4 (Figure 7), indicating that the cementoenamel junction in *Hamipterus* belongs to the overlap interface type rather than the meet or gap interface type (Fehrenbach & Popowics, 2016).

The root surface of the *Hamipterus* tooth exhibits two types of cementum. The first type is acellular cementum

19328494, 0, Downloaded from https://anatomypubs.onlinelibrary.wiley.com/doi/10.1002/ar.25289 by INST VERTEBRATE PALEONTOLOGY, Wiley Online Library on [08/08/2023]. See the Terms and Conditions (https://onlinelibrary.wiley.com/terms-and-conditions) on Wiley Online Library for rules of use; OA articles are governed by the applicable Creative Commons License

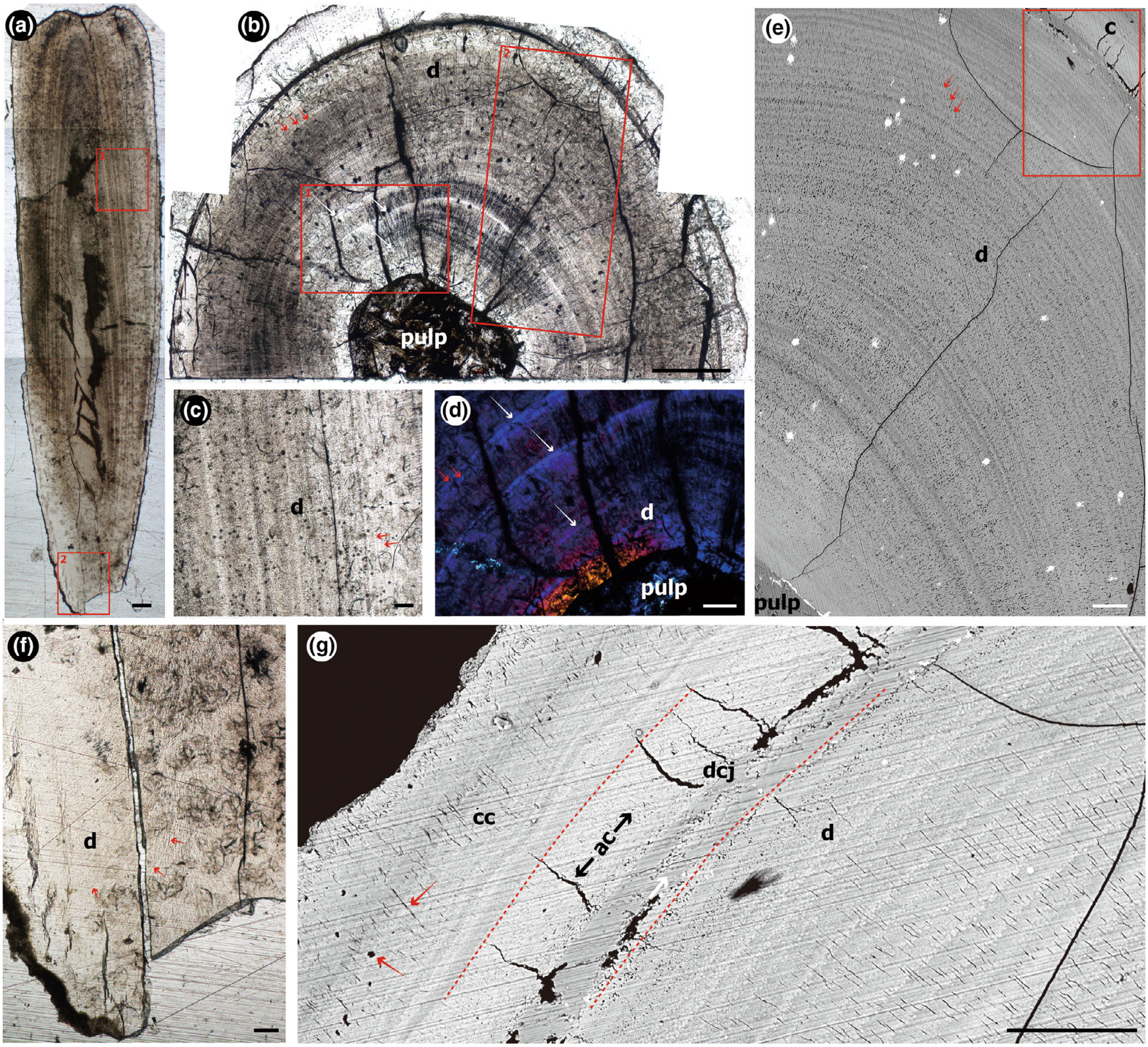

FIGURE 4 Microanatomy of the dental structure in *Hamipterus* (IVPP V 32250.5). (a), (c) and (f) are transmission micrographs of the axial sections. (c) and (f) are close-ups of the No. 1 and No. 2 red boxes in (a), respectively. (b) is transmission micrograph of the transverse thin sections. The polarizing micrograph (d) is a close-up of the No. 1 red box in (b). The SEM micrograph (e) is a close-up of the No. 2 red box in (b). The SEM micrograph (g) is a close-up of the red box in (e) and shows the cementocyte lacunae (red arrows) and the filled matrix (white arrow) during taphonomy inside the acellular cementum layer. Both the short-period von Ebner lines (red arrows in b, c, d, e) and long-period Andresen lines (white arrows in b, d) are clear in the dentine area. (f) shows the tubules curving to the radicular pulp on the basal tooth (red arrows). ac, acellular cementum; c, cementum; cc, cellular cementum; d, dentine; dcj, dentine–cementum junction. Scale bars: a and b = 500 μm, c–g = 100 μm.

(Figures 2c, 4g and 6b,d), which lacks cementocytes and is deposited over the dentine at the dentinocemental junction. The second type is the cellular cementum, similar to that in extant animals (Berkovitz & Shellis, 2017). This outermost layer contains embedded cementocytes (Figure 2d) deposited over the thin layer of acellular cementum adjacent to the dentine (Figure 2c). The appositional growth of cellular cementum is indicated by the presence of lines of arrested growth, which appear as smooth growth rings in the cross-sectional microscopic views (Figures 2c,d and 4g).

Similar to that in other vertebrates, such as the sperm whale, the spring hare, and *Crocodylus* (Berkovitz & Shellis, 2017), the dentine in *Hamipterus* also exhibits

19328494, 0, Downloaded from https://anatomypubs.onlinelibrary.wiley.com/doi/10.1002/ar.25289 by INST VERTEBRATE PALEONANTOLOGY, Wiley Online Library on [08/08/2023]. See the Terms and Conditions (https://onlinelibrary.wiley.com/terms-and-conditions) on Wiley Online Library for rules of use; OA articles are governed by the applicable Creative Commons License

19328494, 0, Downloaded from https://anatomypubs.onlinelibrary.wiley.com/doi/10.1002/ar.25289 by INST VERTEBRATE PALEONANTOLOGY, Wiley Online Library on [08/08/2023]. See the Terms and Conditions (https://onlinelibrary.wiley.com/terms-and-conditions) on Wiley Online Library for rules of use; OA articles are governed by the applicable Creative Commons License

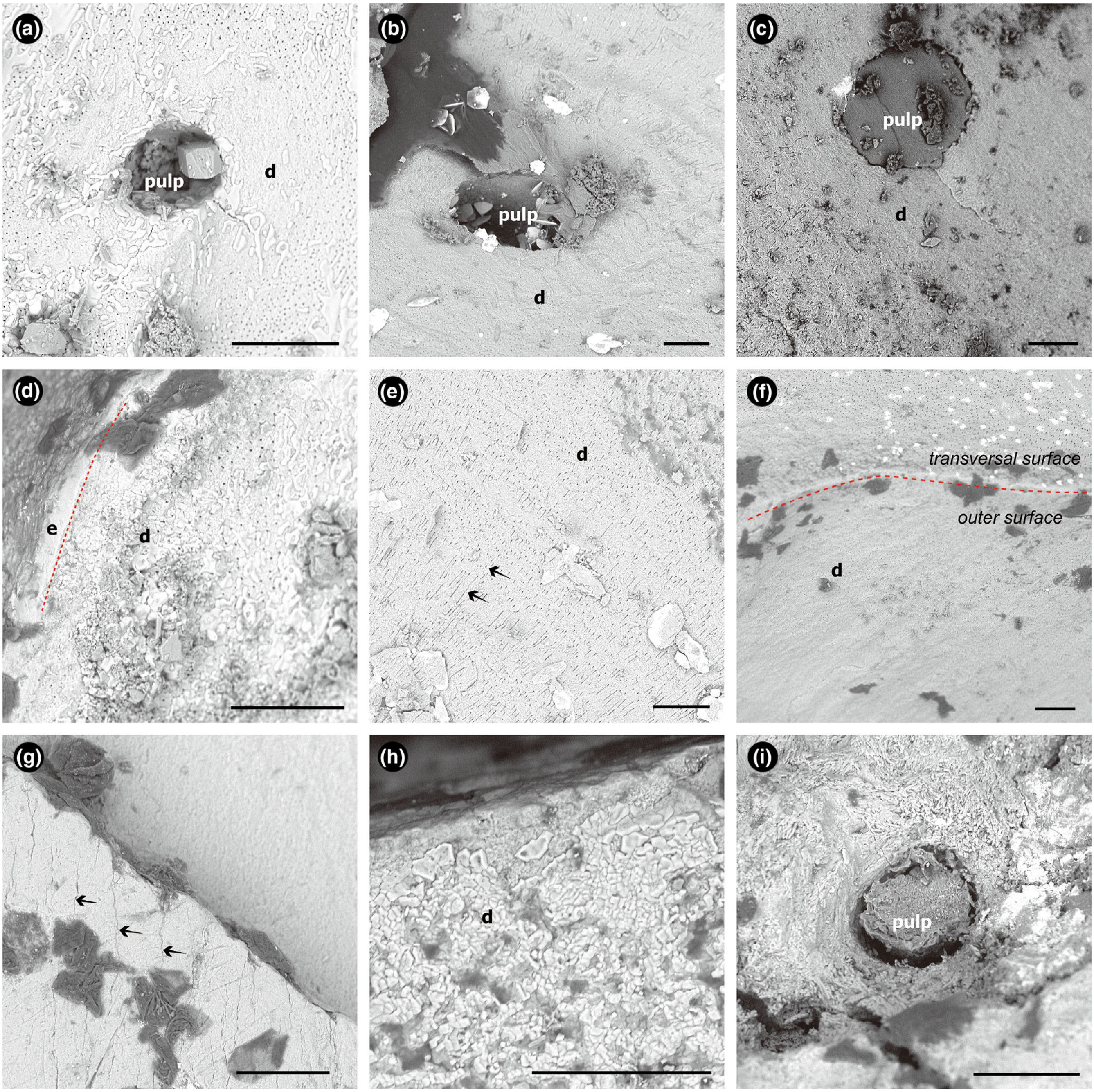

FIGURE 5 SEM micrographs of the surface features on the broken area of the teeth in *Hamipterus*. (a) and (d) are the broken transverse surfaces on the top of the crown in IVPP V 32250.2, showing the coronal pulp surrounded by orthodentine with tubules (a) and a very thin outer layer that belongs to the enamel (d). (b), (c) and e–i are the micrographs taken of IVPP V 32250.1. The size of the slender tunnel of coronal pulp is similar from the middle (c) to the top area (b) of the tooth. The dentine tubules generally show tiny points closer to the outer layer (f) and pulp (a) and short lines in the middle (b and c, black arrow in e) of the tooth crown. The tooth crown surface has numerous small axial cracks (black arrow) and microwear (g). The broken transverse surface in the middle part of the tooth shows lamellar-shaped crystallites on the orthodentine (h). A very small foramen (~60 μm) (i) on the tip of the tooth root connects the radicular pulp of the tooth. d, dentine; e, enamel. All scale bars are equal to 50 μm.

two types of incremental lines: Andresen lines (long periodicity) and von Ebner lines (short periodicity) (Figure 4b,d). Andresen lines reflect periodic variations in the orientation of collagen fibers and are particularly clear under polarizing microscopy (Berkovitz & Shellis, 2017). Between the long-period Andresen lines, short-period von Ebner lines occur (Berkovitz & Shellis, 2017). The von Ebner lines represent a daily

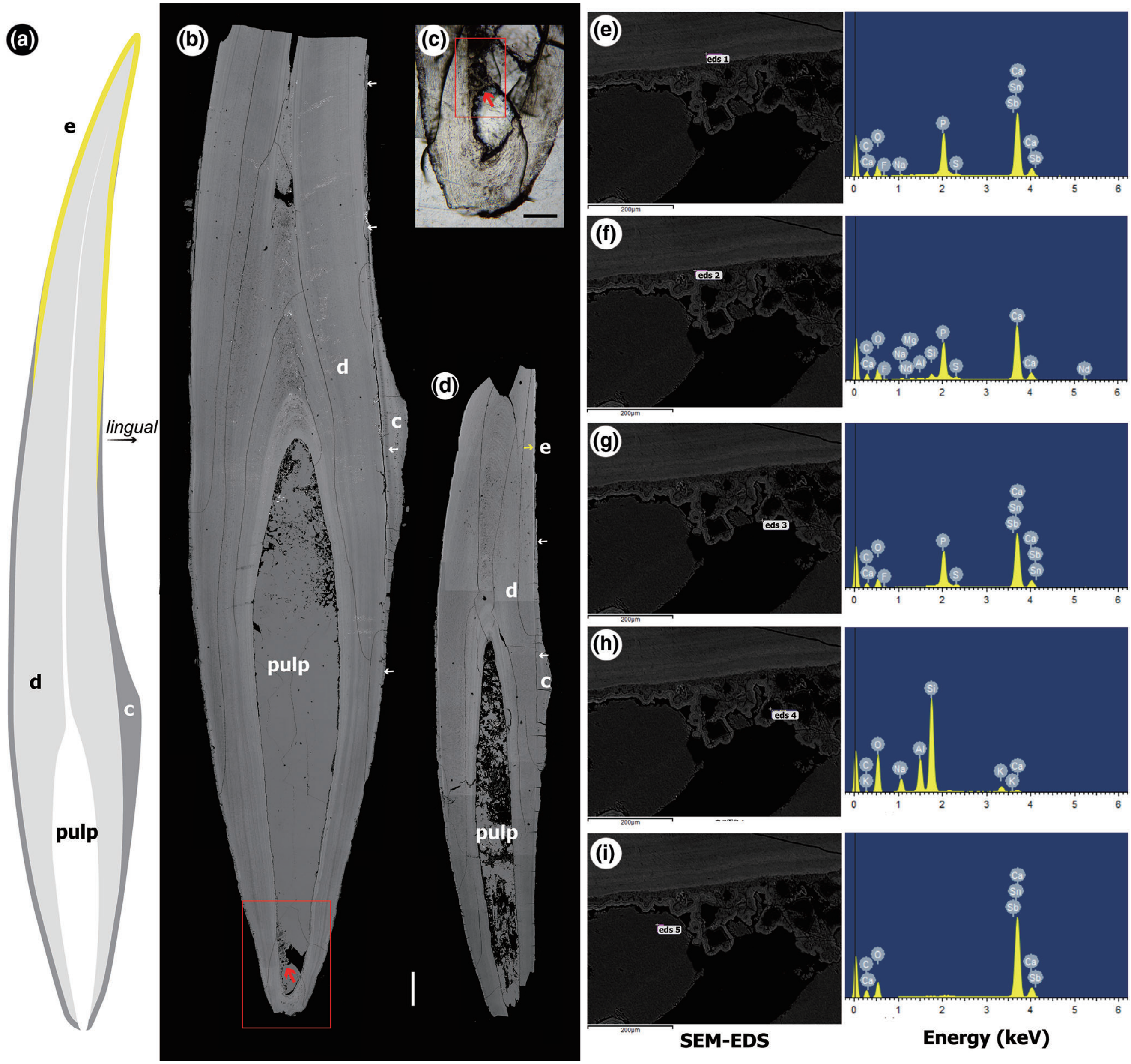

FIGURE 6 Illustration of the *Hamipterus* tooth axial plate and its SEM diagrams and EDS analysis results. (a) is an illustration showing the different dental layers. (b) is an axial thin-section SEM micrograph of IVPP V 32250.3. c is the micrograph close-up from the corresponding area of the red box in (b). (d) is an axial thin-section SEM micrograph of tooth IVPP V 32250.4. (e–i) are the diagrams of SEM–EDS results focused on the corresponding area of the red box in (c). A twist dentine layer are preserved on the radicular pulp surface at the bottom of the root in IVPP V 32250.3 (red arrow in b and c). The preserved continuing outer layers on the lingual side clearly show the acellular cementum layer from the root to the partial crown (white arrow in b and d). The density of the enamel on the inside is slightly higher (yellow arrow in d). c, cementum; d, dentine; e, enamel. Scale bar: b and d = 500 μm, c = 200 μm.

increment of dentine mineralization (Dean, 1998; Erickson, 1996a, 1996b) and can be observed at different distances from each other in all thin sections (Figures 2, 4 and 6). The number of von Ebner lines between Andresen lines ranges from 7 to 15, suggesting potential weekly or monthly periods in *Hamipterus*, although the exact periodicities of these lines require further investigation. In the cross-section of IVPP V 32250.5, the widths of the von Ebner lines vary in the transverse (labiolingual) (16–21 μm) and longitudinal (mesiodistal) sections (13–23 μm). The mean widths of the von Ebner lines are 18.5 μm and 18 μm in these two sections, respectively, and occasionally thinner growth lines (13 μm) appear in the middle of the dentine (Figure 4b). The growth lines around the distal pulp cavity are bent toward the cavity (Figure 6b,d).

19328494, 0, Downloaded from https://anatomypubs.onlinelibrary.wiley.com/doi/10.1002/ar.25289 by INST VERTEBRATE PALEONANTOLOGY, Wiley Online Library on [08/08/2023]. See the Terms and Conditions (https://onlinelibrary.wiley.com/terms-and-conditions) on Wiley Online Library for rules of use; OA articles are governed by the applicable Creative Commons License

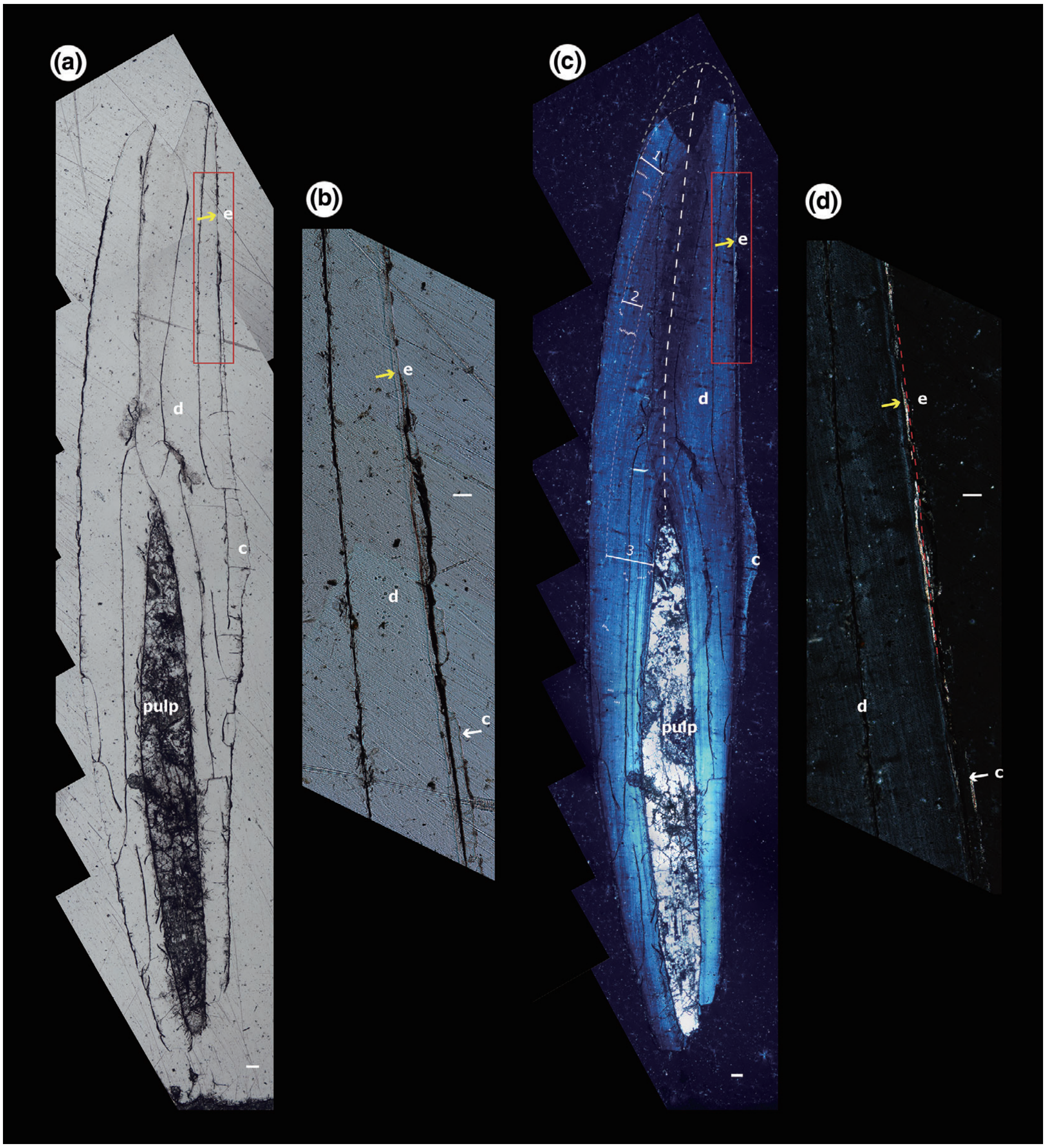

FIGURE 7 Tooth axial micrographs of *Hamipterus* (IVPP V 32250.4). (b) is a close-up of the corresponding area of the red box on its axial thin section (a). The polarizing micrograph (d) is a close-up of the red boxes in (c). c, cementum; d, dentine; e, enamel. The estimated central axis height is indicated with dashed lines in (c). Scale bar: a and c = 100 μm, b and d = 50 μm.

3.3 | Tooth formation time

The number of von Ebner lines from an axial section near the central axis will closely reflect tooth formation (Kosch & Zanno, 2020). However, due to the preciousness of complete fossil teeth, we selected a small tooth (IVPP V 32250.4) that had lost its tip to estimate its formation time based on the estimated central axis. To facilitate accurate counting, we divided it into three stages (Figure 7c). In stage one, 16 von Ebner lines were observed, while in stage two, 18 von Ebner lines were counted. However, not all von Ebner lines were clearly visible in stage three (Figure 7c). We estimate that there are 36 von Ebner lines in Stage, including 9 lines (within the 90 μm unclear areas) estimated from the 10 μm average width of nearby von Ebner lines. Based on the axial section count, approximately 70 von Ebner lines were identified. Considering the estimated height of the central axis, the tooth formation time for this small tooth was estimated to be approximately 80 days (Figure 7c).

3.4 | SEM–EDS analysis

EDS analysis revealed high peaks of calcium and phosphorus in all dental layers (IVPP V 32250.3, 32250.4 and 32251.1). Additionally, the thin cross-section of IVPP V

19328494, 0, Downloaded from https://anatomypubs.onlinelibrary.wiley.com/doi/10.1002/ar.25289 by INST VERTEBRATE PALEONTOLOGY, Wiley Online Library on [08/08/2023]. See the Terms and Conditions (https://onlinelibrary.wiley.com/terms-and-conditions) on Wiley Online Library for rules of use; OA articles are governed by the applicable Creative Commons License

32250.5 exhibits fissures and secondary mineralization in the dentine area (Figure 4e,g). In the thin cross-section of IVPP V 32250.3 (Figure 6e,g), a curved, twisting layer was preserved within the innermost dentine layer on the surface of the radicular pulp (Figure 6b,c). This layer displayed continuity with the dentine layer, apparent under microscopy (Figure 6c), but it appeared darker in image acquired using the Back-scattered Electron Detector (BSE), indicating a distinct composition (Figure 6b,e–i). The EDS results demonstrated similar compositions for this layer and the dentine layer, primarily consisting of Ca, P and O with small peaks attributed to C, S, and F (Figure 6e,g). Although this irregularly curved and folded layer resembles the plicidentine found in the basal portions of teeth in *Latimeria* and some reptiles (Kearney & Rieppel, 2006; Meunier et al., 2015), it is not extensively folded vertically as in plicidentine (Kearney & Rieppel, 2006; Meunier et al., 2015). Therefore, this irregularly curved dental layer may represent a unique feature specific to IVPP V 32250.3 or possibly remnants from the last mineralization stage of orthodentine.

4 | COMPARISONS AND DISCUSSION

It is understandable that due to taphonomy, the crown part of fossil teeth is less frequently preserved than other parts. As the diagenetic minerals in bones, this taphonomical process may also lead to the fragile nature of fossil teeth. Furthermore, the enamel is very thin and does not have a sufficiently high density to preserve or protect the dentin. We observed that the enamel is poorly preserved in the fossil teeth of *Hamipterus*. The thickness of the enamel layer identified is approximately 25 μm, which is similar to the general thickness of the enamel of? *Santanadactylus* sp. but much thinner than that of crocodylians (∼360 μm) and dinosaurs, including the spinosaur (55–90 μm) (Vidovic, 2010). This outer layer covers almost half of the functional tooth, slightly more than in? *Santanadactylus* sp. (Vidovic, 2010), and differs from the enamel layer of dinosaurs (e.g., Button et al., 2017; D'Emic et al., 2013; D'Emic et al., 2019; Ősi et al., 2022; Sereno et al., 2007) and crocodylians (Erickson, 1996a, 1996b). Despite the enamel layer exhibiting increased density from the outer surface inward (Figure 6d), its density is still not obviously higher than that of the acellular cementum, as revealed through SEM (Figure 6d).

Compared with the dental calculus, the outer layer of *Hamipterus* teeth with small rounded lacuna clusters is likely the cellular cementum (Figures 2c, 4g and 6b,d). Although some dental calculus may also cover the root area and preserve a variety of biomolecules or their lacunae (Velsko & Warinner, 2017; Warinner et al., 2014), it lacks the presence of regular parallel growth lines in the same anatomical position across different teeth, as observed in the cellular cementum. The thick, cellular cementum, found mostly on the lingual side of the crown-root area of the tooth in *Hamipterus*, has hardly been noted in other pterosaurs, dinosaurs, and crocodylians (e.g., Enax et al., 2013; Heckeberg & Rauhut, 2020; Vidovic, 2010). This cellular cementum responds to tooth wear and movement (Fehrenbach & Popowics, 2016), so its development indicates that the teeth of *Hamipterus* are well stabilized in the alveoli.

The regular periodicity of the Andresen lines corresponds to increments of dentine apposition over periods of 7–15 days in *Hamipterus*. This estimated time is closer to the periods observed in some extant mammals, such as humans and great apes (6–10 days), monkeys (4–5 days), and proboscideans (13–14 days) (Dean & Scandrett, 1996). In comparison, *Crocodylus* exhibits long-period lines, with 15–35 von Ebner lines (Berkovitz & Shellis, 2017). The mean von Ebner line increment width (VEIW) data from the transverse sections can still be used for comparisons between different clades. The short-period lines (von Ebner lines) represent daily increments of growth of approximately 18.5 μm in *Hamipterus*, slightly higher than that of crocodylians (16 μm) (Erickson, 1996a, 1996b). These values are higher than those of *Edmontonia* (13.9 μm) and *Pinacosaurus grangeri* (15.7 μm) (Hill et al., 2015), closer to that of *Hungarosaurus* (15–19 μm) but lower than that of *Mochlodon* (33.55 μm) (Ősi et al., 2022). Given the variation in VEIW observed among dinosaurs, it is important to investigate whether this degree of daily deposition of tooth formation varies among the pterosaurs. This exploration can help determine if the widths of daily deposition of the tooth are related to the variety of tooth morphotypes and diets among pterosaurs.

Ontogeny barely impacts the mean VEIW in alligator (Kosch & Zanno, 2020), and similarly, the mean VEIW does not vary significantly with tooth size in *Hamipterus* (Table 1). Based on our estimation, the formation time of a small tooth (2.7 mm width in the mesiodistal widest area) in *Hamipterus* is approximately 80 days. Therefore, even if we double the formation time for a larger tooth with double the size, *Hamipterus* would still require a shorter tooth formation time than theropods (293–359 days, e.g., D'Emic et al., 2019; Heckeberg & Rauhut, 2020) and crocodylians (Erickson, 1996a, 1996b). The dentin deposition and the thin short enamel layer may both contribute to the shortened development time of teeth in *Hamipterus*.

No replacement tooth preserved with antecedent teeth in different individuals at various developmental

19328494, 0, Downloaded from https://anatomypubs.onlinelibrary.wiley.com/doi/10.1002/ar.25289 by INST VERTEBRATE PALEONTOLOGY, Wiley Online Library on [08/08/2023]. See the Terms and Conditions (https://onlinelibrary.wiley.com/terms-and-conditions) on Wiley Online Library for rules of use; OA articles are governed by the applicable Creative Commons License

stages of *Hamipterus* has been found. Instead, there is either the distolingual replacement of the tooth as in *Coloborhynchus* (Fastnacht, 2008) or the circular resorption of *Eudimorphodon* (Wild, 1978), similar to in alligator (Wu et al., 2013). While *Pterodaustro* exhibits a distinct pattern of tooth replacement, it indicates that dental variation and complexity are related to changes in the spatial distribution of tissues rather than the occurrence of novel tissues in the evolution of the clades (Cerda & Codorniú, 2023). Therefore, further investigation and the discovery of specific preserved materials are required to determine the patterns of tooth replacement in *Hamipterus*. Furthermore, this will allow the estimation of the tooth replacement rate of *Hamipterus*.

5 | CONCLUSION AND PERSPECTIVES

Our study focuses on the detailed dental microstructure analysis of *Hamipterus*, and all of the specimens in this study were discovered in the Lower Cretaceous Shengjinkou Formation of Hami, Xinjiang, China. The results indicate that the conical-shaped root of *Hamipterus* teeth contains a spindle-spaced radicular pulp, which narrows into a small tunnel (100–140 μm in diameter) on the crown. The enamel in *Hamipterus* is very thin and only covers nearly half the height of the total functional tooth, similar to that of ?*Santanadactylus* sp. The thin, small, covered area and the low density of the enamel might be related to the fragile and fragmentary fossil tooth preservation in *Hamipterus*. The acellular cementum surrounding the dentine not only covers the whole root but also extends to parts of the tooth crown. The thickest cellular cementum layer covers the cervical root surface. Moreover, the thick cellular cementum layer stabilizes the tooth in the alveolus. Two types of incremental lines on the dentine are clearly shown in *Hamipterus*, which are von Ebner lines and Andresen lines. The periodicity of Andresen lines is approximately 7–15 days in the teeth of *Hamipterus*, similar to that in some mammals. Investigations of the incremental lines in the small teeth of *Hamipterus* showed relatively short tooth formation times (∼80 days).

AUTHOR CONTRIBUTIONS

He Chen: Data curation; formal analysis; investigation; methodology; software; validation; visualization; writing – original draft. **Zhiheng Li:** Methodology; supervision; writing – review and editing. **Shunxing Jiang:** Investigation; writing – review and editing. **Qian Wu:** Formal analysis; writing – review and editing. **Yanxin Gong:** Writing – review and editing. **Xufeng Zhu:** Investigation; writing – review and editing. **Xiaolin Wang:** Project administration; supervision; writing – review and editing.

ACKNOWLEDGMENTS

We are grateful to Mr. Long Xiang, Mr. Hongjiao Zhou and Dr. Yang Li for their help during the fieldwork in Hami. We thank Mr. Xun Jin (IVPP), Dr. Hong Pang, Dr. Tong Bao, Dr. Binlan Zhang, Dr. Yanyan Chu, Mr. Zuqi Mai and Mr. Jiadong Yin (all from SYSU) for their help in using the SEM and contacting the polarizing microscope. We are also grateful to Dr. Paul Rummy, Dr. Changfu Zhou and an anonymous reviewer for their constructive comments, and to the Chief Editor Dr. Heather Smith for the English editing, which greatly improved this manuscript. This research was supported by the National Natural Science Foundation of China (42288201, 42072028 and 41572020), the Strategic Priority Research Program (B) of CAS (XDB26000000) and the Youth Innovation Promotion Association of Chinese Academy of Sciences (2019075).

ORCID

He Chen https://orcid.org/0000-0003-0259-0676
Qian Wu https://orcid.org/0000-0001-7646-8329

REFERENCES

Benton, M. J., Bouaziz, S., Buffetaut, E., Martill, D., Ouaja, M., Soussi, M., & Trueman, C. (2000). Dinosaurs and other fossil vertebrates from fluvial deposits in the lower cretaceous of southern Tunisia. *Palaeogeography, Palaeoclimatology, Palaeoecology*, *157*(3–4), 227–246.

Berkovitz, B. K., & Shellis, R. P. (2017). *The teeth of non-mammalian vertebrates*. Academic Press.

Bestwick, J., Unwin, D. M., Butler, R. J., Henderson, D. M., & Purnell, M. A. (2018). Pterosaur dietary hypotheses: A review of ideas and approaches. *Biological Reviews*, *93*, 2021–2048. https://doi.org/10.1111/brv.12431

Brink, K., Reisz, R., LeBlanc, A., Chang, R., Lee, Y., Chiang, C., Huang, T., & Evans, D. (2015). Developmental and evolutionary novelty in the serrated teeth of theropod dinosaurs. *Scientific Reports*, *5*(1), 12338.

Button, K., You, H., Kirkland, J. I., & Zanno, L. (2017). Incremental growth of therizinosaurian dental tissues: Implications for dietary transitions in Theropoda. *PeerJ*, *5*, e4129.

Cerda, I. A., & Codorniú, L. (2023). Palaeohistology reveals an unusual periodontium and tooth implantation in a filter-feeding pterodactyloid pterosaur, *Pterodaustro guinazui*, from the lower cretaceous of Argentina. *Journal of Anatomy*, 1–11. https://doi.org/10.1111/joa.13878

Chiappe, L. M., Kellner, A. W. A., Rivarola, D., Davila, S., & Fox, M. (2000). Cranial morphology of *Pterodaustro guinazui* (Pterosauria: Pterodactyloidea) from the lower cretaceous of Argentina. *Contributions in Science*, *483*, 1–19.

Dalla Vecchia, F. M. (2004). An *Eudimorphodon* (Diapsida, Pterosauria) specimen from the Norian (late Triassic) of north-eastern Italy. *Gortania*, *25*, 47–72.

19328494, 0, Downloaded from https://anatomypubs.onlinelibrary.wiley.com/doi/10.1002/ar.25289 by INST VERTEBRATE PALEONANTOLOGY, Wiley Online Library on [08/08/2023]. See the Terms and Conditions (https://onlinelibrary.wiley.com/terms-and-conditions) on Wiley Online Library for rules of use; OA articles are governed by the applicable Creative Commons License

Dean, M. C. (1998). Comparative observations on the spacing of short-period (von Ebner's) lines in dentine. *Archives of Oral Biology*, *43*(12), 1009–1021.

Dean, M. C., & Scandrett, A. E. (1996). The relation between long-period incremental markings in dentine and daily cross-striations in enamel in human teeth. *Archives of Oral Biology*, *41*(3), 233–241.

D'Emic, M. D., O'Connor, P. M., Pascucci, T. R., Gavras, J. N., Mardakhayava, E., & Lund, E. K. (2019). Evolution of high tooth replacement rates in theropod dinosaurs. *PLoS One*, *14*(11), e0224734.

D'Emic, M. D., Whitlock, J. A., Smith, K. M., Fisher, D. C., & Wilson, J. A. (2013). Evolution of high tooth replacement rates in sauropod dinosaurs. *PLoS One*, *8*(7), e69235.

Enax, J., Fabritius, H.-O., Rack, A., Prymak, O., Raabe, D., & Epple, M. (2013). Characterization of crocodile teeth: Correlation of composition, microstructure, and hardness. *Journal of Structural Biology*, *184*(2), 155–163.

Erickson, G. M. (1996a). Daily deposition of dentine in juvenile alligator and assessment of tooth replacement rates using incremental line counts. *Journal of Morphology*, *228*(2), 189–194.

Erickson, G. M. (1996b). Incremental lines of von Ebner in dinosaurs and the assessment of tooth replacement rates using growth line counts. *Proceedings of the National Academy of Sciences*, *93*(25), 14623–14627.

Fastnacht, M. (2001). First record of *Coloborhynchus* (Pterosauria) from the Santana formation (lower cretaceous) of the Chapada do Araripe, Brazil. *Paläontologische Zeitschrift*, *75*(1), 23–36.

Fastnacht, M. (2008). Tooth replacement pattern of *Coloborhynchus robustus* (Pterosauria) from the lower cretaceous of Brazil. *Journal of Morphology*, *269*(3), 332–348. https://doi.org/10.1002/jmor.10591

Fehrenbach, M. J., & Popowics, T. (2016). *Illustrated dental embryology, histology, and anatomy* (4th ed.). Elsevier Health Sciences.

Fiorillo, A. R., & Currie, P. J. (1994). Theropod teeth from the Judith River formation (upper cretaceous) of south-Central Montana. *Journal of Vertebrate Paleontology*, *14*(1), 74–80. https://doi.org/10.1080/02724634.1994.10011539

Fröbisch, N. B., & Fröbisch, J. (2006). A new basal pterosaur genus from the upper Triassic of the northern calcareous Alps of Switzerland. *Palaeontology*, *49*(5), 1081–1090.

Gong, Y., Wang, Y., Wang, Y., Mao, F., Bai, B., Wang, H., Li, Q., Jin, X., Wang, X., & Meng, J. (2020). Dietary adaptations and palaeoecology of Lophialetidae (Mammalia, Tapiroidea) from the Eocene of the Erlian Basin, China: Combined evidence from mesowear and stable isotope analyses. *Palaeontology*, *63*(4), 547–564.

Heckeberg, N. S., & Rauhut, O. W. (2020). Histology of spinosaurid dinosaur teeth from the Albian-Cenomanian of Morocco: Implications for tooth replacement and ecology. *Palaeontologia Electronica*, *23*(3), 1–18.

Hill, R. V., D'Emic, M. D., Bever, G. S., & Norell, M. A. (2015). A complex hyobranchial apparatus in a cretaceous dinosaur and the antiquity of avian paraglossalia. *Zoological Journal of the Linnean Society*, *175*(4), 892–909.

Kearney, M., & Rieppel, O. (2006). An investigation into the occurrence of plicidentine in the teeth of squamate reptiles. *Copeia*, *2006*(3), 337–350.

Kellner, A. W. A., & Mader, B. J. (1997). Archosaur teeth from the cretaceous of Morocco. *Journal of Paleontology*, *71*(3), 525–527.

Kosch, J. C. D., & Zanno, L. E. (2020). Sampling impacts the assessment of tooth growth and replacement rates in archosaurs: Implications for paleontological studies. *PeerJ*, *8*, e9918. https://doi.org/10.7717/peerj.9918

Kundanati, L., D'Incau, M., Bernardi, M., Scardi, P., & Pugno, N. M. (2019). A comparative study of the mechanical properties of a dinosaur and crocodile fossil teeth. *Journal of the Mechanical Behavior of Biomedical Materials*, *97*, 365–374.

Li, Y., Luo, W., Yang, Y., Jiang, S., & Wang, X. (2021). A preliminary study of the weathering mechanism of fossilized cretaceous *Hamipterus* bones. *Science China Earth Sciences*, *64*(3), 458–469.

Li, Z., Wang, C. C., Wang, M., Chiang, C. C., Wang, Y., Zheng, X., Huang, E. W., Hsiao, K., & Zhou, Z. (2020). Ultramicrostructural reductions in teeth: Implications for dietary transition from non-avian dinosaurs to birds. *BMC Evolutionary Biology*, *20*(1), 46.

Martill, D. M., Frey, E., Tischlinger, H., Mäuser, M., Rivera-Sylva, H. E., & Vidovic, S. U. (2023). A new pterodactyloid pterosaur with a unique filter-feeding apparatus from the late Jurassic of Germany. *PalZ*, *97*, 383–424. https://doi.org/10.1007/s12542-022-00644-4

Meunier, F. J., Mondéjar-Fernández, J., Goussard, F., Clément, G., & Herbin, M. (2015). Presence of plicidentine in the oral teeth of the coelacanth Latimeria chalumnae Smith 1939 (Sarcopterygii; Actinistia). *Journal of Structural Biology*, *190*(1), 31–37.

Ősi, A. (2011). Feeding-related characters in basal pterosaurs: Implications for jaw mechanism, dental function and diet. *Lethaia*, *44*(2), 136–152.

Ősi, A., Barrett, P. M., Evans, A. R., Nagy, A. L., Szenti, I., Kukovecz, Á., Magyar, J., Segesdi, M., Gere, K., & Jó, V. (2022). Multi-proxy dentition analyses reveal niche partitioning between sympatric herbivorous dinosaurs. *Scientific Reports*, *12*(1), 20813.

Owen, R. (1845). *Odontography* (vol. 1). Hippolyte Bailliere.

Sánchez-Hernández, B., Benton, M. J., & Naish, D. (2007). Dinosaurs and other fossil vertebrates from the late Jurassic and early cretaceous of the Galve area, NE Spain. *Palaeogeography, Palaeoclimatology, Palaeoecology*, *249*(1–2), 180–215.

Sereno, P. C., Wilson, J. A., Witmer, L. M., Whitlock, J. A., Maga, A., Ide, O., & Rowe, T. A. (2007). Structural extremes in a Cretaceous dinosaur. *PLoS One*, *2*(11), e1230.

Velsko, I. M., & Warinner, C. G. (2017). Bioarchaeology of the human microbiome. *Bioarchaeology International*, *1*(1–2), 86–99.

Vidovic, S. U. (2010). A preliminary analysis of dental microstructure in pterosaurs. *Acta Geoscientica Sinica*, *31*, 70–72.

Wang, X., Kellner, A. W. A., Jiang, S., Cheng, X., Wang, Q., Ma, Y., Paidoula, Y., Rodrigues, T., Chen, H., Saya˜O, J. M., Li, N., Zhang, J., Bantim, R. A. M., Meng, X., Zhang, X., Qiu, R., & Zhou, Z. (2017). Egg accumulation with 3D embryos provides insight into the life history of a pterosaur. *Science*, *358*, 1197–1201.

Wang, X., Kellner, A. W. A., Jiang, S., Wang, Q., Ma, Y., Paidoula, Y., Cheng, X., Rodrigues, T., Meng, X., Zhang, J., Li, N., & Zhou, Z. (2014). Sexually dimorphic tridimensionally

19328494, 0, Downloaded from https://anatomypubs.onlinelibrary.wiley.com/doi/10.1002/ar.25289 by INST VERTEBRATE PALEONANTOLOGY, Wiley Online Library on [08/08/2023]. See the Terms and Conditions (https://onlinelibrary.wiley.com/terms-and-conditions) on Wiley Online Library for rules of use; OA articles are governed by the applicable Creative Commons License

preserved pterosaurs and their eggs from China. *Current Biology*, *24*(12), 1323–1330. https://doi.org/10.1016/j.cub.2014.04.054

Wang, X., Li, Y., Qiu, R., Jiang, S., Zhang, X., Chen, H., Wang, J., & Cheng, X. (2020). Comparison of biodiversity of the early cretaceous pterosaur faunas in China. *Earth Science Frontiers*, *27*(6), 347–364. https://doi.org/10.13745/j.esf.sf.2020.6.19

Warinner, C., Rodrigues, J. F. M., Vyas, R., Trachsel, C., Shved, N., Grossmann, J., Radini, A., Hancock, Y., Tito, R. Y., Fiddyment, S., Speller, C., Hendy, J., Charlton, S., Luder, H. U., Salazar-García, D. C., Eppler, E., Seiler, R., Hansen, L. H., Castruita, J. A. S., … Cappellini, E. (2014). Pathogens and host immunity in the ancient human oral cavity. *Nature Genetics*, *46*(4), 336–344.

Wellnhofer, P. (2003). A late Triassic pterosaur from the northern calcareous Alps (Tyrol, Austria). *Geological Society, London, Special Publications*, *217*(1), 5–22.

Wild, R. (1978). Die Flugsaurier (Reptilia, Pterosauria) aus der Oberen Trias von Cene bei Bergamo, Italien. *Bollettino Della Società Paleontologica Italiana*, *17*(2), 176–256.

Wu, P., Wu, X., Jiang, T.-X., Elsey, R. M., Temple, B. L., Divers, S. J., Glenn, T. C., Yuan, K., Chen, M.-H., Widelitz, R. B., & Cheng-Ming, C. (2013). Specialized stem cell niche enables repetitive renewal of alligator teeth. *Proceedings of the National Academy of Sciences*, *110*(22), E2009–E2018.

Xu, Y., Jiang, S., & Wang, X. (2022). A new istiodactylid pterosaur, *Lingyuanopterus camposi* gen. Et sp. Nov., from the Jiufotang formation of western Liaoning, China. *PeerJ*, *10*, e13819. https://doi.org/10.7717/peerj.13819

Zhou, C., Gao, K., Yi, H., Xue, J., Li, Q., & Fox, R. C. (2017). Earliest filter-feeding pterosaur from the Jurassic of China and ecological evolution of Pterodactyloidea. *Royal Society Open Science*, *4*(2), 160672.

How to cite this article: Chen, H., Li, Z., Jiang, S., Wu, Q., Gong, Y., Zhu, X., & Wang, X. (2023). A preliminary analysis of dental microstructure in *Hamipterus* (Pterosauria, Pterodactyloidea). *The Anatomical Record*, 1–15. https://doi.org/10.1002/ar.25289

19328494, 0, Downloaded from https://anatomypubs.onlinelibrary.wiley.com/doi/10.1002/ar.25289 by INST VERTEBRATE PALEONANTOLOGY, Wiley Online Library on [08/08/2023]. See the Terms and Conditions (https://onlinelibrary.wiley.com/terms-and-conditions) on Wiley Online Library for rules of use; OA articles are governed by the applicable Creative Commons License